INVESTIGATIONS OF THE AUDIBLE NOISE OF INDUCTORS WITH RESPECT TO DIFFERENT FERROMAGNETIC MATERIALS

Gerd Terörde, Jürgen Schneider* and Kay Hameyer

Katholieke Universiteit Leuven, E.E. Dept., Div. ESAT/ELEN
Kardinaal Mercierlaan 94, B-3001 Leuven, BELGIUM
E-mail: gerd.teroerde@esat.kuleuven.ac.be

*Elektroblech Bochum GMBH
Castroper Straße 228, D-44791 Bochum, GERMANY

Abstract — **Fluorescent lamps are one of the most modern light sources. They can be connected to the 230 Vac supply without a transformer. To operate them, an inductor and starter are required only. The main disadvantage of this type of light source is the emitted audible noise of a frequency of 100 Hz. For this phenomenon the inductor is responsible. Electromagnetic forces and magnetostriction are acting on the body of the device causing the sound emission. Here, the audible noise problem is investigated with respect to different ferromagnetic materials and the range of applied flux densities inside the iron core.**

I. INTRODUCTION

The circuit and the current-voltage characteristic of a fluorescent lamp explain the task of the inductor. To operate these kind of lamps the elements from figure 1 are required.

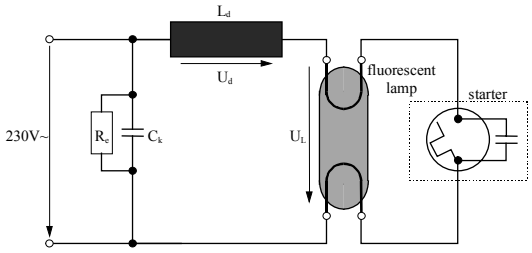

Fig. 1: Fluorescent lamp

A bimetal strip, accommodated in the starter, is bended in consequence of heat, developed by a glimmer, as far as the opposite electrode is contacted and the glimmer is short circuited. The short circuit current, sending out electrons trough thermo emission, is only limited by the reactance of the inductance and the heat spiral of the lamp. After the expiring of the glimmer the bimetal calms, falls back in his original position and breaks the current. This current interrupt causes a high inductive voltage over the inductance, resulting in the ignition of the lamp.

Here, the inductor is studied only. It has to fulfil the following tasks:

- limitation of the short circuit current
- ignition of the lamp
- stabilisation of the current after ignition (Fig. 2)

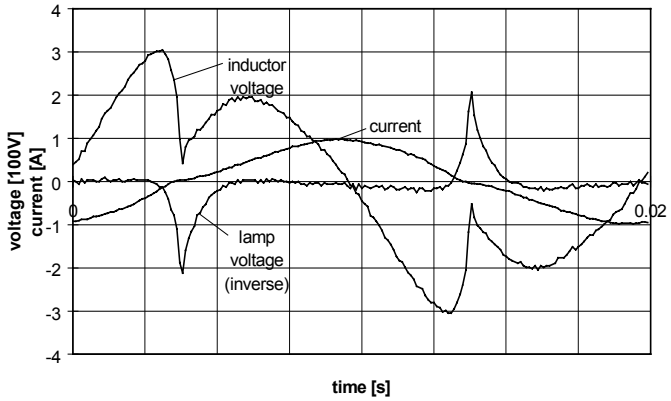

Fig. 2: Current-voltage characteristic

II. MAGNETIC COMPUTATION

To evaluate the electromagnetic field distribution inside the inductor body, the finite element method (FEM) in two dimensions is used. The FEM delivers, in dependence on the current, the magnetic field distribution (Fig. 3) as well as the field energy. The range of magnitude of the magnetic flux density until ignition, and for the rated point of operation of the lamp different ferromagnetic materials are studied.

Based on the symmetry, it is sufficient to model half of the geometry. The studied materials are anisotropic. It has to be distinguished between the angle phi=0°, which describes the rolling direction, and the perpendicular angle phi=90°. To consider the anisotropy of the ferromagnetic material it is important to build subsections in the two dimensional inductor model. These subsections must be linked, as a function of the predominant flux and rolling direction, with the affiliated material characteristics. For more complex systems, the association of the subsections performs a coupled problem, which must be solved in an iterative loop.

The flux direction and the resulting material areas at the rated point of current (I_N=0,67A) are plotted in Fig. 3.

To calculate the resistance of the winding and the losses a coupled thermal computation, considering iron and copper losses, is used. The iron losses are composed of magnetic hysteresis losses and eddy-current losses.

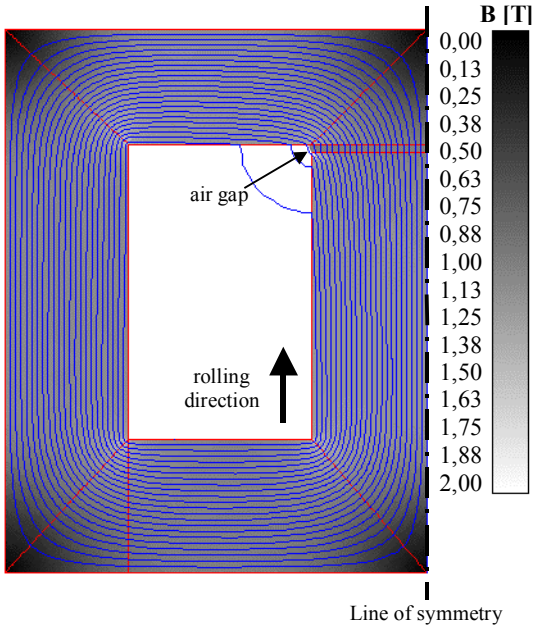

Fig. 3: Magnetic induction at rated current

The overall iron losses are integrated by:

$$P = A\,l\rho \int_B \left([p_V(B)\%A]_{phi=0^\circ} + [p_V(B)\%A]_{phi=90^\circ} \right) dB \quad (1)$$

A is the surface, l the length of the inductor, p_V the specific losses and ρ the density of the material used. The flux density necessary to evaluate (1) is determined by the weighted field distribution (Fig. 4).

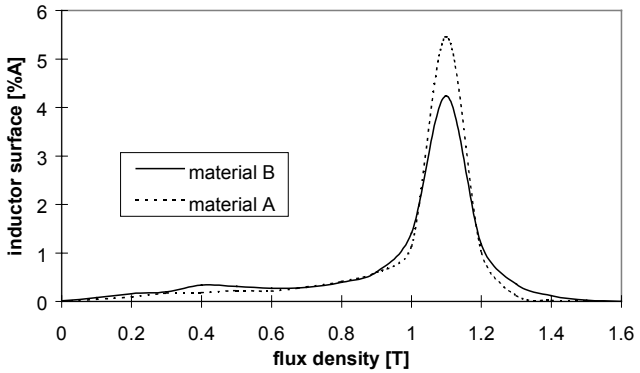

Fig. 4: Percentage of field distribution

With correct linked subsections the results of the magnetic calculation become more realistic. Measurements of the current-voltage characteristic, shown in figure 5, exhibits the great conformity with the FEM calculation .

However, the accuracy of the numerical solution depends also on the accuracy of the input data. The material characteristics are measured results and therefore given with tolerances.

The rated operating point describes the dynamic range of the current. The plotted short circuit point indicates the current, which will be reached by the maximum allowed voltage V_{max}=250V.

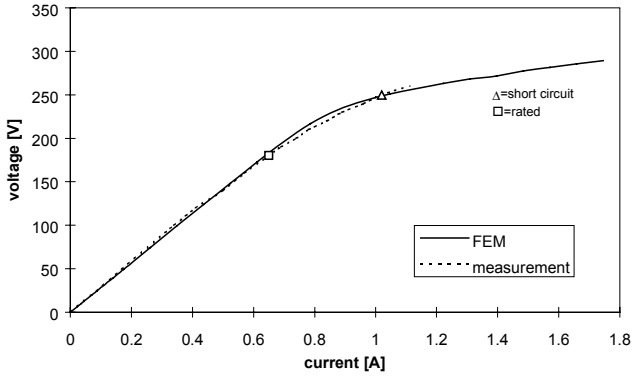

Fig. 5: Measurement compared to FEM solution (material A)

The calculation of the energy in non-linear systems depends on the point of view. For the computation of the stored magnetic energy W_{mag} the local field distribution is required. This magnetic field energy, stored in the inductor system, results from:

$$W_{mag} = \iiint_V \left(\int_B \vec{H} \cdot \vec{dB} \right) \cdot dV \quad (2)$$

Whereas, for the calculation of the flux linkage Ψ another form of energy is necessary. The energy W_{lin} is given by the integral over the coil area about the product of the vector potential A and the current density J. This integral can be interpreted as the energy input of the supply and describes the global system behaviour.

$$W_{lin} = \frac{1}{2\mu_0} \cdot \iiint_V \frac{B^2}{\mu_r} \cdot dV = \frac{1}{2} \cdot \iiint_V \vec{A} \cdot \vec{J} \cdot dV \quad (3)$$

$$\Psi = \frac{2 \cdot n \cdot W_{lin}}{\theta} = \frac{2 \cdot W_{lin}}{i} \quad (4)$$

However, this energy form does not yield the real existing energy stored in the system. In the case of linearity the above described energy forms are identically. A comparison delivers a reliable declaration over the dynamic range, in which the inductance of the iron-cored inductor behaves linearly. In figure 6 these energy forms are shown for two different materials as a function of the current.

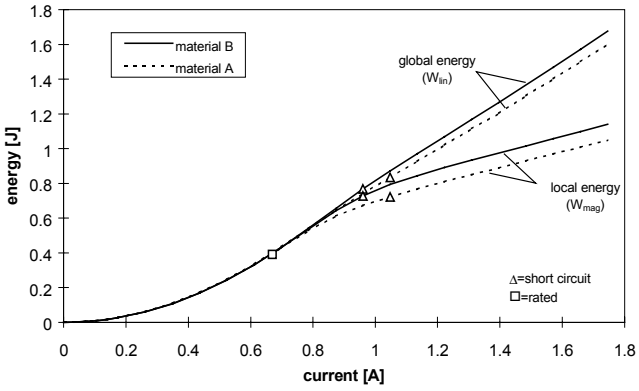

Fig. 6: Energy stored in the system

The self inductance L can be determined from the above described energy forms W_{lin} and W_{mag} as follows:

$$W = \frac{1}{2} \cdot L \cdot I^2 \qquad (5)$$

Following this, for the non-linear operation of the system two different definitions of the self-inductance are given [1].

Here, the inductance's of the ferromagnetic cored inductor, based on the global energy form, are computed as a function of the current (Fig. 7).

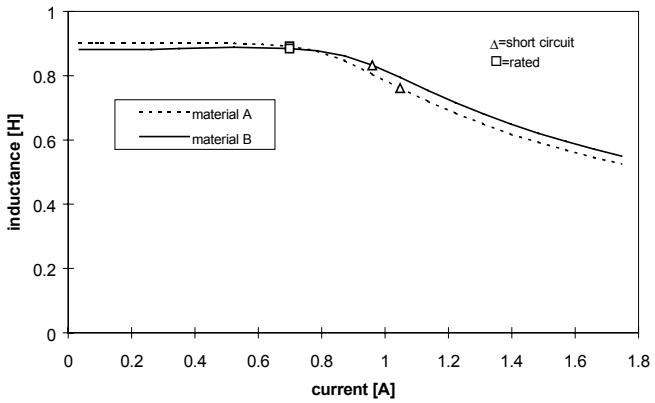

Fig. 7: Inductance

III. FORCE AND DEFORMATION

An air gap is present in the magnetic circuit to adjust the inductance of the inductor during manufacturing. This enables electromagnetic normal forces (Fig. 8), as a function of the current, to deform the body of the inductor. Here, it is assumed that the inductor is freely suspending in space without coupling to a housing.

The surface forces are obtained by the numerical field computation by using the Maxwell stress tensor. The local stress is computed at all points of the bounding surface and then summed via a surface integral to find the normal forces F_N in the air gap:

$$F_N = \frac{1}{\mu_0} z_0 \cdot \int_c \left(B_y^2 - \frac{1}{2} \cdot |B|^2 \right) dx \,,\ z_0 = \text{length;} \qquad (6)$$

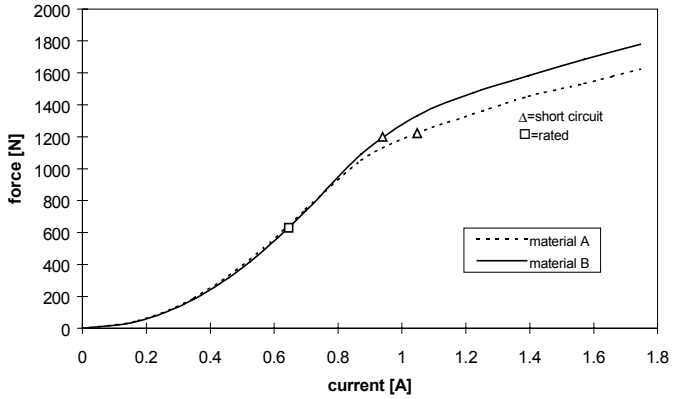

Fig. 8: Electromagnetic force

The force characteristics in figure 8 deludes into thinking that larger forces are developed by the material B. But this is an indication of larger linearity. Because of the non-linearity, the same voltage causes a greater current and thus a greater electromagnetic force in the inductor with the material A.

The calculated normal forces are used in the mechanical structural computation to calculate the maximum deformation of the inductor body. The deformation Δy by rated operation is illustrated in figure 9 with a magnifying factor of 1500. The maximum deformation due to electromagnetic forces is 0,62µm.

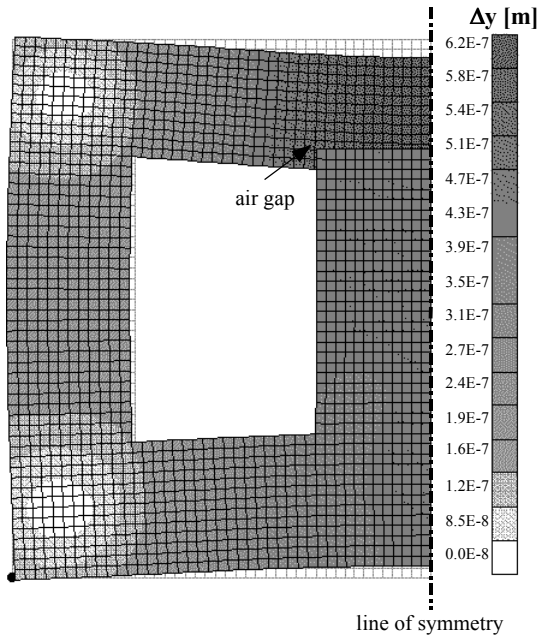

Fig. 9: Deformation due to electromagnetic forces (rated operation)

Additionally, the internal frequency of the system plays an important part for the calculation of the deformation. If the internal frequency is distinctly higher than the frequency of the exciting force, it results in inductor vibrations with a relative small amplitude. The elongation of the device and the forces acting on it are nearly in synchronism, i.e. there is no displacement between the excitation and the deformation.

However, the calculation of the internal frequency is proved to be very difficult. Here, the internal frequency of the inductor is estimated by means of a simplified model. The geometry is modelled out of rectangular bars. The internal frequencies f_n of a rectangular bar with thickness d and length l can be calculated according to the following relation [4]:

$$f_n = \frac{s_n^2 \cdot d}{2 \cdot \pi \cdot \sqrt{12} \cdot l^2} \sqrt{\frac{E}{\rho}} \,,\ \rho = \textit{density},\ s_n = \textit{coefficient;} \qquad (7)$$

The coefficient s_n results out of the way of fixing and the ordinal number. The minimum internal frequencies for the inductor studied, amounts to about $f_1 \approx 19$kHz. This frequency is much higher than the stimulating frequency f_s=100Hz.

Therefore, the force and the deformation are in phase and the deformation of the device can be determined with the help of a static calculation.

The phenomenon of magnetostriction is strongly depending on the range of flux density inside the magnetic core. The

deformation λ, caused by the magnetostriction under influence of small magnetic flux densities, shows a squared dependence on the magnetic induction (Fig.10):

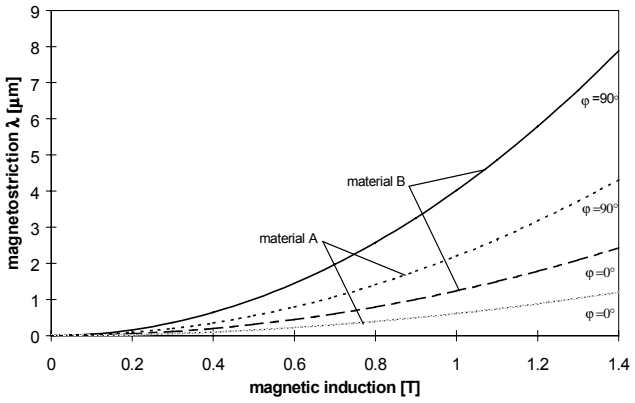

Fig. 10: Measured characteristics of magnetostriction

Furthermore, for the calculation of the magnetostrictive effects, the rolling direction must be considerated due to the anisotropic behaviour. The magnetostriction depends strongly on the direction of the magnetic flux. During a magnetisation of the tin package vertical to the rolling direction appears a much higher length variation, than during a magnetisation in rolling direction.

Expansion diagrams containing the electromagnetic field parameters and the magnetostrictive characteristics (Fig. 10) are used to estimate the deformation of the material. The deformation Δy due to the magnetostriction at rated operation is shown in figure 11 with a magnifying factor of 15000 in this case. The maximal deformation is 72nm.

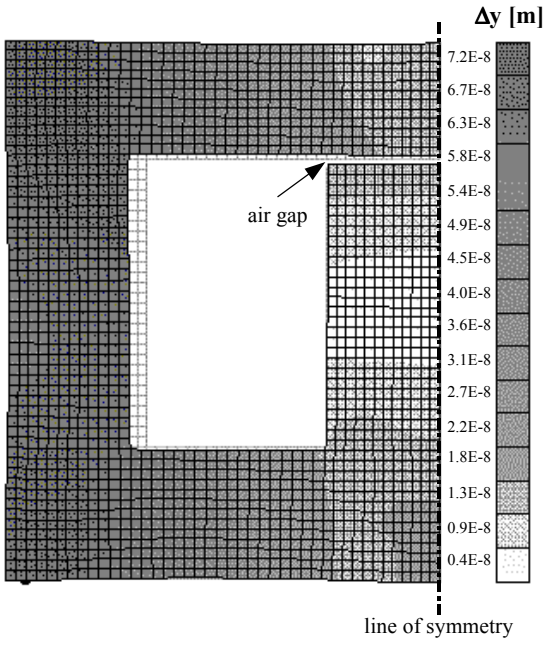

Fig. 11: Deformation due to magnetostriction (rated operation)

IV. AUDIBLE NOISE CALCULATION

To study the sound or audible noise behaviour of the inductor device with respect to different ferromagnetic materials, the behaviour of the magnetic core of the device is calculated.

Hence, the power of sound of the audible noise is estimated for the inductor only, no coupling to the housing of the lamp is considered. The geometrical dimensions of the device are in the range of some centimetres, certainly much shorter than the fundamental wave length of the emitted noise. Therefore, the results, obtained by the computation of the mechanical deformation, are referred to an acoustic single body source to estimate the power of the emitted audible noise.

The sound intensity can be determined by means of two spherical radiator models. The simplest model is the zero order radiator. This behaviour is caused by the magnetostriction. The whole surface oscillates simultaneously outwards and inwards. The system changes periodically its volume and consequently, radiates spherical sound waves.

The deformation due to electromagnetic forces builds a sound system of second order. The opposite surfaces oscillate against each other, while the volume stays nearly constant.

The sound pressure in the distance r to the source can be analytically estimated with the following equation [4]:

$$p = \frac{1}{4\pi r}\left(\rho S \frac{d\upsilon}{dt}\right)e^{j(wt-kr)}\ ,\ \rho = density,\ S = surface \quad (8)$$

The velocity parameter ν for the deformation due to electromagnetic forces exceeds the value ν due to magnetostriction about one order of magnitude. Because of the larger magnetostrictive active surface, the larger velocity will be equalised, so that the audible noise level, resulting out of magnetostriction and electromagnetic forces, are of the same order.

V. CONCLUSIONS

To estimate the audible noise of inductors used in fluorescent lamps with respect to different ferromagnetic materials used for the inductor, electromagnetic and structural mechanical field computations are employed. For both types of field problems the finite element method is used. The mathematical model of a single body spherical source is used to estimate the audible noise level emitted by the magnetic core. A comparison with measurements supports the methods used. With this approach, shape optimisations of the inductor are possible to minimise the sound level, subject to geometrical constraints such as length, overall volume, range of flux density distribution, etc.

ACKNOWLEDGEMENT

The authors are grateful to the Belgian Fonds voor Wetenschappelijk Onderzoek Vlaanderen for its financial support of this work and the Belgian Ministry of Scientific Research for granting the IUAP No. P4/20 on Coupled Problems in Electromagnetic Systems. The authors are thankful to Prof. D. Vandepitte for the possibility to use the structural FEM package FEMAP.

REFERENCES

[1] Lowther, D.A. and Silvester, P.P.: Computer aided design in magnetics, Springer Verlag, 1985.
[2] Michalowsky, L. et al: Magnettechnik, Grundlagen und Anwendungen, Fachbuchverlag Leipzig, 1993.

[3] Belmans, R.: Recent major developments in cae and vibrations and audible noise analysis of rotating electrical machines, Garant, 1994.
[4] Veit, I.: Technische Akustik, Vogel Verlag ,1974.